Quantum Mechanics of the Cooper Pair Box: From Charge Qubit to Transmon

Harry Luo

Physics 531 May 5, 2025

Introduction

The Cooper Pair Box (CPB) is a foundational superconducting circuit element whose quantum behavior, governed by the **interplay** between charging energy (E_C) and Josephson energy (E_J), forms the basis for prevalent qubit designs [2]. Its dynamics are described by the Hamiltonian:

$$\hat{H} = 4E_C(\hat{N} - n_g)^2 - E_J^{(1)} \cos\hat{\phi} - \frac{E_J^{(2)}}{2}\cos(2\hat{\phi}) \tag{1}$$

where $\hat{N}$ is the number operator for excess Cooper pairs on a superconducting island, $\hat{\phi}$ is the conjugate phase difference operator ($[\hat{\phi}, \hat{N}] = i$, with $\hbar = 1$), and n_g is the tunable gate charge offset. This paper explores the quantum mechanics of this system in the limiting regimes defined by the ratio E_J/E_C, connects these regimes to the operation of charge and transmon qubits, and analyzes their key properties based on the solutions derived in Appendix A.

Limiting Regimes and Qubit Properties

In the charging dominated regime ($E_C \gg E_J^{(1)}, E_J^{(2)}$), the system favors eigenstates $|N\rangle$ with definite Cooper pair numbers (Appendix A.1). Near degeneracies, such as at the $n_g = 1/2$ charge frustration point, the Josephson coupling $E_J^{(1)}$ mixes the degenerate $|0\rangle$ and $|1\rangle$ states. This creates a two-level system, the **charge qubit**, whose energy levels exhibit an avoided crossing, as shown in Figure 2. A defining characteristic of the charge qubit is its extreme sensitivity to n_g, illustrated by the sharp transition in ground state charge probability shown in Figure 1. This sensitivity makes it highly vulnerable to charge noise.

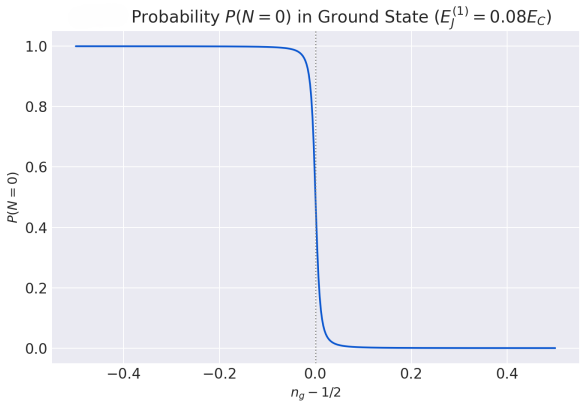

Figure 1: Ground state probability $P(N = 0)$ near $n_g = 1/2$ for $E_J^{(1)} = 0.08E_C$, highlighting the charge qubit's sensitivity to n_g. Calculation details in Appendix A.1.

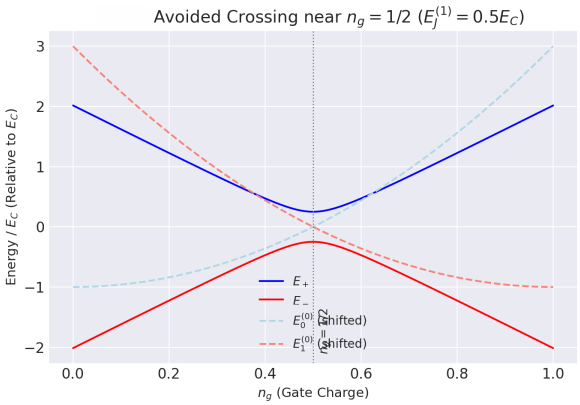

Figure 2: Avoided crossing of the lowest two energy levels near the $n_g = 1/2$ degeneracy point, calculated using the effective 2×2 Hamiltonian for $E_J^{(1)} = 0.5E_C$. The minimum gap is $E_J^{(1)}$. Derivation in Appendix A.1.

In the opposite Josephson dominated regime ($E_J^{(1)}, E_J^{(2)} \gg E_C$, with $n_g = 0$), the phase ϕ becomes localized near the potential minimum [1]. The system is well-approximated as an anharmonic oscillator (Appendix A.2). Phase localization leads to charge number delocalization, meaning the charge state is highly uncertain. The ground state charge variance $\Delta N^2 = \frac{1}{2X}$ (where $X = \sqrt{8E_C/(E_J^{(1)} + 2E_J^{(2)})}$) becomes large, as shown in Figure 3. Furthermore, the potential's anharmonicity ensures non-equidistant energy levels ($E_1 - E_0 \neq E_2 - E_1$), with $\alpha_{anh} \approx -E_C$ (derived in Appendix A.2), which is vital for qubit addressability.

A specific case ($n_g = 0, E_J^{(1)} = E_J, E_J^{(2)} = E_J^2/(4E_C)$) admits an exact ground state solution (Appendix A.3). Its probability density (Appendix Fig. 8) clearly shows the transition from delocalized phase (charge-like, low E_J/E_C) to localized phase (transmon-like, high E_J/E_C).

Interpretation: Charge vs. Transmon Qubits

The distinct behaviors in the limiting regimes of the Cooper Pair Box Hamiltonian naturally lead to two types of superconducting qubits [1,2]. In the charging-dominated regime ($E_C \gg E_J$), the **charge qubit** is formed, typically using the lowest two charge states $|0\rangle$ and $|1\rangle$. Its primary drawback, however, is extreme sensitivity to fluctuations in the gate charge n_g.

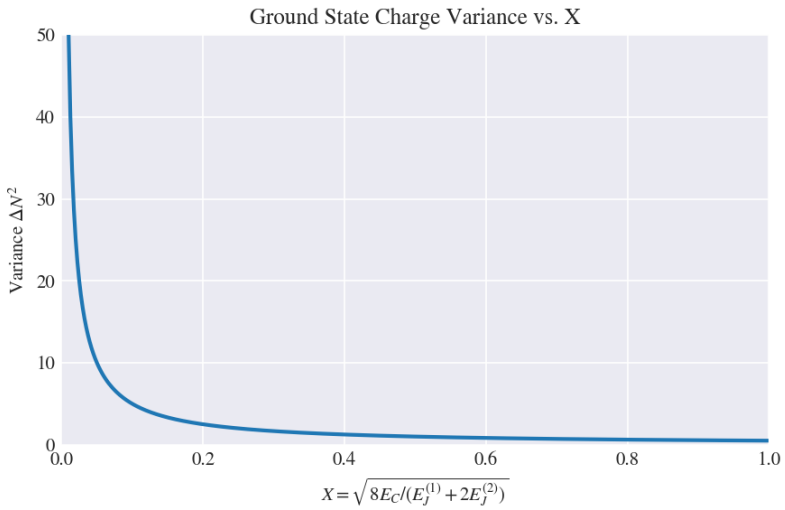

Figure 3: Ground state charge variance $\Delta N^2 = 1/(2X)$ vs $X = \sqrt{8E_C/(E_J^{(1)} + 2E_J^{(2)})}$. Large ΔN^2 in the transmon limit (small X) signifies charge delocalization, key to noise immunity. Calculation in Appendix A.2.

As clearly shown by the sharp transition in the ground state probability (Figure 1) around the $n_g = 1/2$ operating point, small variations in n_g significantly alter the qubit's energy splitting (Figure 2), making it highly susceptible to environmental charge noise.

Conversely, the **transmon qubit** operates deep in the Josephson-dominated regime ($E_J \gg E_C$). Its defining characteristic is a significantly suppressed sensitivity to charge noise. This immunity arises because the quantum state becomes delocalized over many charge numbers, leading to a large charge variance ($\Delta N^2 \gg 1$, Figure 3). Consequently, the qubit's energy levels become exponentially insensitive to n_g, scaling as $\sim e^{-\sqrt{8E_J/E_C}}$ [1]. This effectively averages out the effect of charge fluctuations, providing crucial protection against decoherence, as schematically illustrated by the flat energy bands in Figure 5.

While charge insensitivity is paramount, a practical qubit also requires **anharmonicity**—non-equidistant energy level spacing—to allow selective control of the qubit transition ($0 \leftrightarrow 1$) without exciting higher levels ($1 \leftrightarrow 2$, etc.). The Josephson cosine potential inherently provides this. As calculated from the subleading corrections in the $E_J \gg E_C$ limit (Appendix A.2), the anharmonicity $\alpha_{anh} = (E_2 - E_1) - (E_1 - E_0)$ is finite and approximately equal to $-E_C$. This non-zero α_{anh} ensures the distinct transition frequencies necessary for high-fidelity qubit operations.

The design of an effective transmon therefore involves managing the trade-off between

maximizing charge insensitivity (favoring large E_J/E_C) and maintaining sufficient anharmonicity (which is roughly constant at $-E_C$ in this regime). Figure 4 perfectly encapsulates this critical relationship. Panel (a) demonstrates that the anharmonicity α quickly saturates near the required value of $-E_C$ for $E_J/E_C \gtrsim 10$. Panel (b) simultaneously shows the desired exponential decrease in charge dispersion (the sensitivity to n_g). Together, these plots illustrate how operating at a sufficiently large ratio (e.g., E_J/E_C in the range 20-100 [2]) allows the transmon to achieve substantial noise immunity while preserving the essential anharmonicity for control, fulfilling the design goals implicit in the project requirements (parts b.v and d).

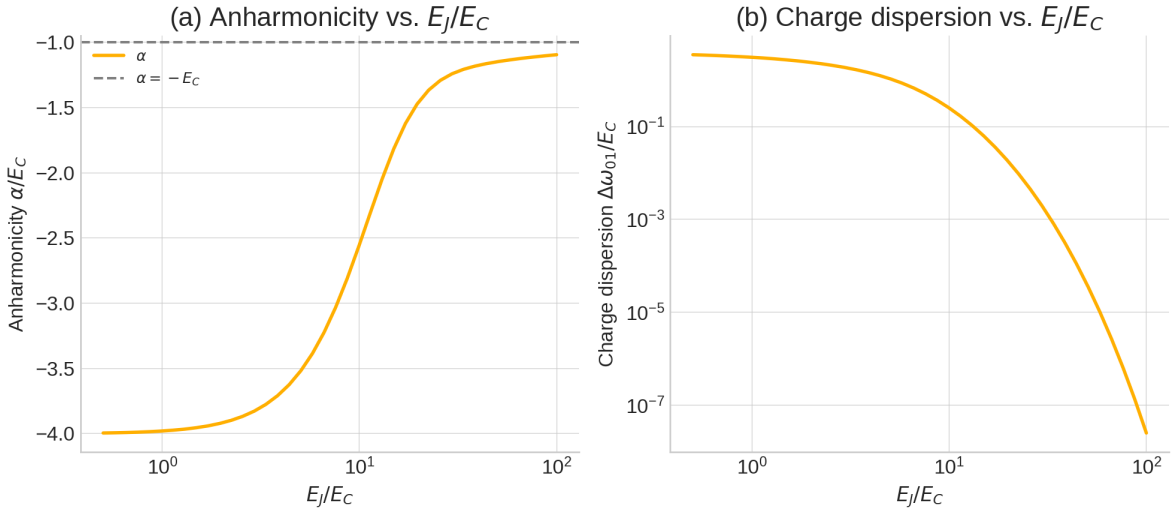

Figure 4: Trade-off between anharmonicity and charge dispersion as a function of the energy ratio E_J/E_C. (a) Anharmonicity $\alpha = (E_2 - E_1) - (E_1 - E_0)$ rapidly approaches the asymptotic value $\alpha \approx -E_C$, sufficient for selective driving. (b) Charge dispersion $\Delta\omega_{01}$ (representing n_g sensitivity) decays exponentially $\propto \exp[-\sqrt{8E_J/E_C}]$ (trend from [1]), enabling noise immunity.

Conclusion

The E_J/E_C ratio fundamentally governs the Cooper Pair Box's quantum behavior, dictating the tradeoff between charge sensitivity and phase localization. The charge qubit regime ($E_C \gg E_J$) suffers from charge noise, while the transmon regime ($E_J \gg E_C$) achieves noise resilience through charge delocalization. This resilience, combined with the essential anharmonicity provided by the Josephson potential, makes the transmon a robust and widely implemented superconducting qubit architecture.

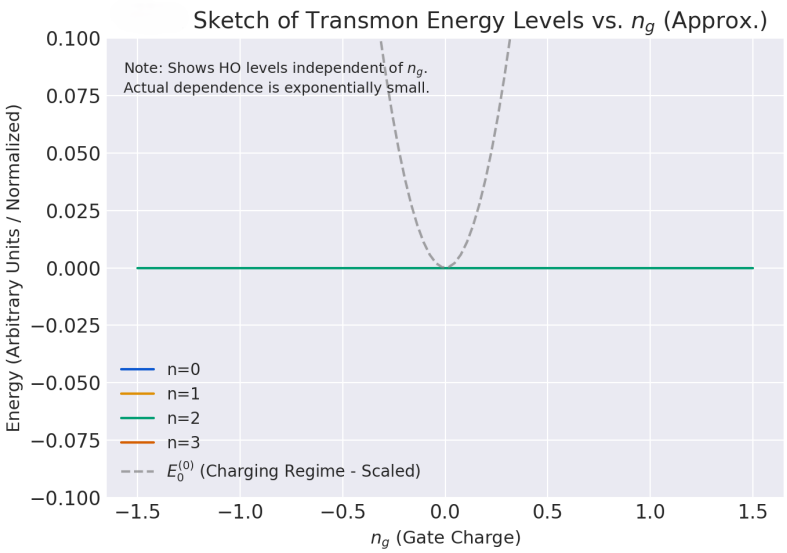

Figure 5: Sketch comparing the flat (charge-insensitive) energy levels of the transmon ($E_J \gg E_C$) with the parabolic (charge-sensitive) levels of the charge qubit regime.

References

[1] J. Koch, T. M. Yu, J. Gambetta, A. A. Houck, D. I. Schuster, J. Majer, A. Blais, M. H. Devoret, S. M. Girvin, and R. J. Schoelkopf, "Charge-insensitive qubit design derived from the Cooper pair box," *Physical Review A* **76**, 042319 (2007).

[2] M. Kjaergaard, M. E. Schwartz, J. Braumüller, P. Krantz, J. I.-J. Wang, S. Gustavsson, and W. D. Oliver, "Superconducting Qubits: Current State of Play," *Annual Review of Condensed Matter Physics* **11**, 369–395 (2020).

A Detailed Calculations

Here we provide the detailed derivations supporting the results presented in the main text, following the structure of the project requirements. We use units where $\hbar = 1$.

A.1 Part (a): Charging Dominated Regime ($E_C \gg E_J^{(1)}, E_J^{(2)}$)

a.i) Eigenstates, Eigenvalues, and Probability Density ($E_J^{(1,2)} = 0$)

The Hamiltonian is $\hat{H}_0 = 4E_C(\hat{N} - n_g)^2$. Eigenstates are $|N\rangle$ ($\hat{N}|N\rangle = N|N\rangle, N \in \mathbb{Z}$). Eigenvalues:

$$E_N^{(0)}(n_g) = 4E_C(N - n_g)^2 \tag{2}$$

These levels are plotted in Figure 6. The eigenfunction $\psi_N(\phi) = \frac{1}{\sqrt{2\pi}} e^{iN\phi}$ yields uniform phase probability density $p_N(\phi) = 1/(2\pi)$.

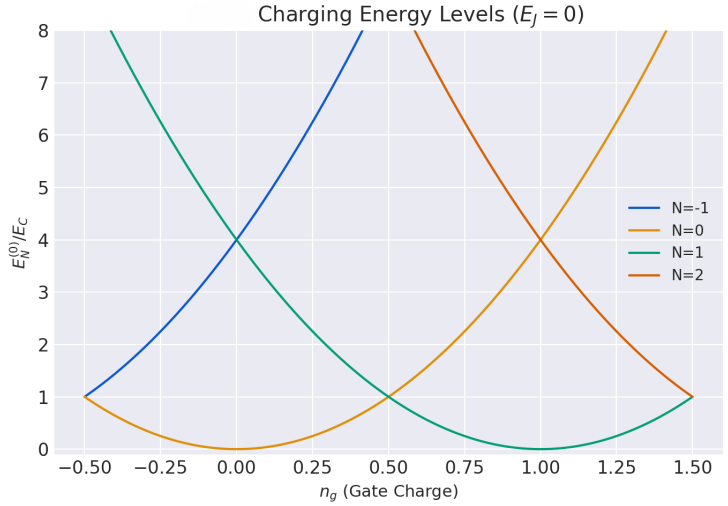

Figure 6: Charging energy levels $E_N^{(0)}/E_C$ versus n_g for $E_J = 0$.

a.ii) Perturbation Theory Correction at $n_g = 0$

Perturbation $V = -E_J^{(1)} \cos\hat{\phi} - \frac{E_J^{(2)}}{2} \cos(2\hat{\phi})$. First-order correction $E_0^{(1)} = 0$. Second-order correction $E_0^{(2)} = \sum_{N \neq 0} \frac{|\langle N|V|0\rangle|^2}{E_0^{(0)} - E_N^{(0)}}$. Using matrix elements $\langle \pm 1|V|0\rangle = -E_J^{(1)}/2$ and

$\langle \pm 2|V|0\rangle = -E_J^{(2)}/4$:

$$E_0^{(2)} = -\frac{(E_J^{(1)})^2}{8E_C} - \frac{(E_J^{(2)})^2}{128E_C} \tag{3}$$

This standard perturbation approach breaks down near degeneracies (half-integer n_g), where the perturbation's effect is strongest.

a.iii) Charge Qubit near $n_g = 1/2$

In the subspace $\{|0\rangle, |1\rangle\}$ near $n_g = 1/2$, the effective Hamiltonian (subtracting $E_C I$) is $H_{\text{eff}} \approx \epsilon_0 \hat{\sigma}_z - \frac{E_J^{(1)}}{2}\hat{\sigma}_x$, where $\epsilon_0 = 4E_C(n_g - 1/2)$. Eigenvalues $E_\pm = \pm\sqrt{\epsilon_0^2 + (E_J^{(1)}/2)^2}$, show an avoided crossing (plotted in Figure 2 in the main text). Ground state (E_-) probability in state $|0\rangle$:

$$P(N=0) = \frac{1}{2}\left(1 - \frac{\epsilon_0}{\sqrt{\epsilon_0^2 + (E_J^{(1)}/2)^2}}\right) \tag{4}$$

This is plotted in Figure 1 in the main text.

A.2 Part (b): Josephson Dominated Regime ($E_J^{(1)}, E_J^{(2)} \gg E_C$, $n_g = 0$)

b.i) Harmonic Oscillator Approximation: Levels and Wavefunctions

Expanding $V(\phi) = -E_J^{(1)}\cos\phi - \frac{E_J^{(2)}}{2}\cos(2\phi)$ around $\phi = 0$ yields $V(\phi) \approx V(0) + \frac{1}{2}k\phi^2$, with $V(0) = -E_J^{(1)} - E_J^{(2)}/2$ and $k = E_J^{(1)} + 2E_J^{(2)}$. $\hat{H} \approx V(0) + 4E_C\hat{N}^2 + \frac{1}{2}k\hat{\phi}^2$ describes a HO with mass $m^* = 1/(8E_C)$ and frequency $\omega = \sqrt{8E_C k}$. Levels: $E_n^{(HO)} = V(0) + \omega(n + 1/2)$. Wavefunctions $\psi_n^{(HO)}(\phi)$ involve Hermite polynomials H_n and width $\alpha = \left(\frac{k}{8E_C}\right)^{1/4}$. First three explicit forms:

$$\psi_0^{(HO)}(\phi) = (\alpha^2/\pi)^{1/4} e^{-\alpha^2\phi^2/2}$$
$$\psi_1^{(HO)}(\phi) = (\alpha^2/\pi)^{1/4}\sqrt{2}\alpha\phi e^{-\alpha^2\phi^2/2}$$
$$\psi_2^{(HO)}(\phi) = (\alpha^2/\pi)^{1/4}\frac{1}{\sqrt{2}}(2(\alpha\phi)^2 - 1)e^{-\alpha^2\phi^2/2}$$

b.ii) Probability Density Plot

The probability densities $p_n(\phi) = |\psi_n^{(HO)}(\phi)|^2$ for $n = 0, 1, 2$ are plotted in Figure 7, using $\alpha^2 = 10$ as required for $E_C = (E_J^{(1)} + 2E_J^{(2)})/800$.

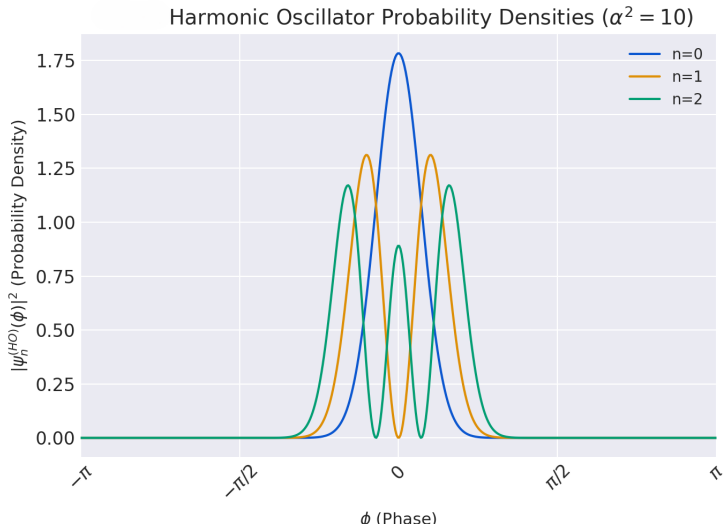

Figure 7: Approximate HO probability densities $p_n(\phi)$ for $n = 0, 1, 2$ with $\alpha^2 = 10$.

b.iii) Charge Expectation Value and Variance

Ground state average $\langle \hat{N} \rangle_0 = 0$. Variance $\Delta N^2 = \langle \hat{N}^2 \rangle_0$. From $\langle KE \rangle_0 = 4E_C \langle \hat{N}^2 \rangle_0$ and $\langle KE \rangle_0 = \omega/4$ (HO ground state): $\langle \hat{N}^2 \rangle_0 = \frac{\omega}{16E_C}$. Standard deviation $\Delta N = \sqrt{\frac{\omega}{16E_C}}$. With $X = \sqrt{8E_C/k}$:

$$\Delta N = \sqrt{\frac{1}{2X}}, \quad \Delta N^2 = \frac{1}{2X} \tag{5}$$

The variance ΔN^2 is plotted in Figure 3 in the main text.

b.iv) Subleading Correction to Energy Levels

Perturbation $V_{pert} = -\frac{E_J^{(1)} + 8E_J^{(2)}}{24} \hat{\phi}^4$. First-order correction $E_n^{(1)} = \langle n | V_{pert} | n \rangle$. Using $\langle n | \hat{\phi}^4 | n \rangle = (\frac{4E_C}{\omega})^2 (6n^2 + 6n + 3)$:

$$E_n^{(1)} = -C(6n^2 + 6n + 3), \quad \text{where} \quad C = \frac{E_C(E_J^{(1)} + 8E_J^{(2)})}{12(E_J^{(1)} + 2E_J^{(2)})} \tag{6}$$

Corrections for first three levels: $E_0^{(1)} = -3C$, $E_1^{(1)} = -15C$, $E_2^{(1)} = -39C$.

b.v) Interpretation: Are Levels Equidistant?

The anharmonicity is $\alpha_{anh} = (E_2 - E_1) - (E_1 - E_0) \approx E_2^{(1)} - 2E_1^{(1)} + E_0^{(1)} = (-39C) - 2(-15C) + (-3C) = -12C$.

$$\alpha_{anh} = -E_C \frac{E_J^{(1)} + 8E_J^{(2)}}{E_J^{(1)} + 2E_J^{(2)}} \tag{7}$$

Since $\alpha_{anh} \neq 0$, the energy levels are not equidistant. The spacing decreases with n ($\alpha_{anh} < 0$). This allows selective driving of the $0 \leftrightarrow 1$ qubit transition.

A.3 Part (c): Exactly Solvable Case ($E_J^{(1)} = E_J, E_J^{(2)} = E_J^2/(4E_C)$)

With $n_g = 0$ and the specified $E_J^{(1,2)}$, the exact ground state energy is $E_0 = -E_J^2/(8E_C)$. The normalized probability density is:

$$p(\phi) = \frac{\exp(\frac{E_J}{2E_C}\cos\phi)}{2\pi I_0(E_J/(2E_C))} \tag{8}$$

where I_0 is the modified Bessel function. This is plotted in Figure 8 for the required E_J/E_C values. Comparison: This E_0 matches $E_0^{(2)}$ from Appendix A.1 if $E_J^{(2)} = 0$. It differs from the HO approximation $E_0^{(HO)} \approx -(E_J + \frac{E_J^2}{8E_C}) + \sqrt{2E_C E_J + E_J^2}$.

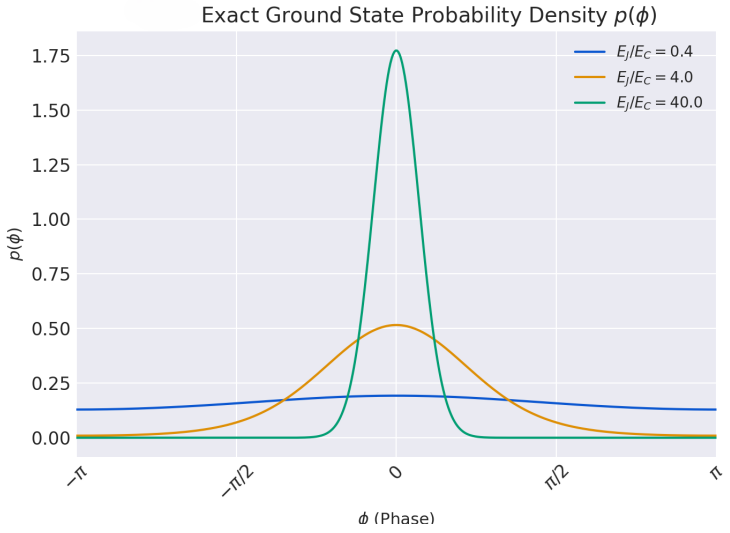

Figure 8: Exact ground state probability density $p(\phi)$ for $E_J/E_C = 0.4, 4.0, 40.0$.